

Quaternion-Hadamard Network: A Novel Defense Against Adversarial Attacks with a New Dataset

Vladimir Frants, Sos Again, *Fellow, IEEE*

Abstract—This paper addresses the vulnerability of deep-learning models designed for rain, snow, and haze removal, which, despite enhancing the image quality in adverse weather, are susceptible to adversarial attacks that compromise their effectiveness. Traditional defenses such as adversarial training and model distillation often require extensive retraining, making them costly and impractical for real-world deployment. While denoising and superresolution techniques can help with image classification models, they impose high computational demands and introduce visual artifacts that hinder image processing tasks. We propose a model-agnostic defense against first-order white-box adversarial attacks using the Quaternion-Hadamard Network (QHNet) to tackle these challenges. White-box attacks are complicated to defend against since attackers have full access to the model’s architecture, weights, and training procedures. Our defense introduces the Quaternion Hadamard Denoising Convolutional Block (QHDCB) and the Quaternion Denoising Residual Block (QDRB), leveraging polynomial thresholding. QHNet incorporates these blocks within an encoder-decoder architecture, enhanced by feature refinement, to effectively neutralize adversarial noise. Additionally, we introduce the Adversarial Weather Conditions Vision Dataset (AWCVD), created by applying first-order gradient attacks on state-of-the-art weather removal techniques in scenarios involving haze, rain streaks, and snow. Using PSNR and SSIM metrics, we demonstrate that QHNet significantly enhances the robustness of low-level computer vision models against adversarial attacks compared with state-of-the-art denoising and superresolution techniques. The source code and dataset will be released alongside the final version of this paper.

Index Terms—Hadamard Transform, Quaternion Neural Network, Computer Vision, Image Processing

I. INTRODUCTION

The rise of autonomous driving and advanced surveillance systems underscores the importance of robustness and efficiency in adverse weather conditions. State-of-the-art rain, snow, and haze removal techniques can significantly improve image quality, enhancing the visibility of details [1], [2]. However, relying on deep learning, these models remain vulnerable to adversarial attacks [3]. Such attacks introduce small perturbations, invisible to the human eye, to deceive the target model, potentially causing critical vulnerabilities in the entire system [4], [5].

Adversarial attacks are broadly categorized into white-box and black-box, based on the attacker’s knowledge of the target model. In a white-box attack, which is the focus of this paper, the attacker has complete access to the model, including its architecture, weights, and training data, making it a more challenging scenario.

One of the foundational methods for generating adversarial examples is the Fast Gradient Sign Method (FGSM), introduced by Goodfellow et al. in 2014 [6]. FGSM manipulates the input image by using the model’s gradients to maximize the loss, creating an adversarial example. The Projected Gradient Descent (PGD) method refines this approach by iteratively adjusting the input while ensuring the perturbations remain within a defined boundary, further challenging the model’s robustness [7].

Early research demonstrated that adversarial attacks could transfer between different CNN architectures, making them a persistent threat across multiple models [8]. Recently, transformers have emerged as a popular alternative in low-level computer vision tasks, but their susceptibility to adversarial attacks has become a growing concern [9]. Aldahdooh et al.’s studies indicate that vanilla Vision Transformers (ViTs) and hybrid ViTs exhibit varying degrees of robustness against different L_p -norm-based attacks compared to CNNs [10]. Mahmood et al. further highlighted that adversarial examples do not readily transfer between CNNs and transformers, underscoring the need for defense strategies adaptable to different model architectures [11].

Current state-of-the-art defense techniques, such as adversarial training and model distillation, though effective, are resource-intensive and often impractical for real-world deployment. Adversarial training, which incorporates adversarial examples into the training process, significantly boosts robustness but at a steep computational cost—often up to ten times the initial training cost [12]. Other defense strategies focus on input transformations that remove adversarial perturbations before the data is fed into the model. Techniques such as JPEG compression, bit-depth reduction, inpainting, and image quilting have been proposed as potential defenses, offering varying degrees of success [13]–[18]. Denoising and superresolution methods have also been explored as defense mechanisms. These approaches assume that image processing methods can learn a generic mapping function that transforms adversarially perturbed images back onto the manifold of natural images [19]. Deep convolutional neural networks (CNNs) are typically used to learn this mapping function, effectively modeling the distribution of unperturbed image data. However, high-end superresolution and denoising techniques are computationally expensive and prone to introducing artifacts, making them unsuitable for low-level computer vision tasks [20]. Furthermore, most of the research in this area is focused on image classification and does not adequately address the restoration quality of the processed images.



Fig. 1. Effects of adversarial attacks on weather removal methods. (a) inability to remove the weather condition; (b) severe artifacts; (c) severe image alteration.

Various approaches to designing compact and efficient image processing models have been proposed, including attention mechanisms, lightweight architectures like MobileNets, knowledge distillation, learning in the transform domain, quaternion neural networks (QNN), capsule networks, and binary neural networks [21]-[25]. Nevertheless, the robustness of these techniques against adversarial attacks remains an unexplored topic. We will focus on using HNNs due to their valuable properties, including their ability to handle complex data representations and their robustness against certain types of noise. Also, QNNs are ideal for processing color images by treating color as a single entity and encoding relationships between channels using the Hamilton product. This approach improves learning dynamics and robustness while reducing the number of parameters by up to four times. It enhances deep learning models' representation and learning capabilities, particularly for spatial transformations and multidimensional signal processing, and increases performance and reduces the number of parameters by up to four times. This may enhance learning dynamics and robustness to adversarial attacks [27].

The defense of image processing methods against adversarial attacks requires several key considerations. First, the defense strategy must be training-free and model-agnostic, meaning it should not require retraining and should work across different models without modifications. Second, it should minimize distortions to preserve image quality. Third, computationally expensive processes, such as superresolution, should be avoided to ensure applicability in resource-constrained environments. Finally, the defense must be robust, preventing attackers from efficiently bypassing it. We aim to develop a practical and effective defense mechanism for image processing models by focusing on these criteria.

This paper introduces a model-agnostic defense strategy against white-box adversarial attacks using the Quaternion-Hadamard Network (QHNet). Unlike existing methods that require retraining or impose high computational costs, QHNet is designed to be both efficient and effective, ensuring robustness without sacrificing image quality. QHNet combines the strengths of Quaternion Neural Networks (QNNs) and the Walsh-Hadamard Transform (WHT) [32]. The WHT, an orthogonal transform based on simple additions and subtractions, makes QHNet highly suitable for resource-limited environments [28]. QHNet introduces the Quaternion Hadamard Denoising Convolutional Block (QHDCB) and the Quaternion Denoising

TABLE I
DEFENCES AGAINST ADVERSARIAL ATTACKS

Method	Training	Artifacts	Effectiveness
Distillation [29], [12], [4]	Yes	Low	High
JPEG compression [13]	No	Low	Moderate
Input transformations [14]	No	Moderate	High
Pixel deflection [15]	No	Moderate	High
Inpainting [16]	No	High	High
Superresolution [19]	No	High	Low

Residual Block (QDRB), integrated within an encoder-decoder framework and refined by a Quaternion Feature Aggregation and Refinement Block (QFARB).

This architecture effectively removes adversarial noise, producing perturbation-free images that are safe for processing by weather removal methods. Additionally, the paper introduces a polynomial thresholding layer in the Hadamard transform domain to improve noise suppression and prevent gradient-based attacks due to its non-differentiable nature.

The main contributions of this work are:

1. A Quaternion-Hadamard Neural Network (QHNet) that defends low-level computer vision models without requiring retraining or adversarial data augmentation;
2. A novel polynomial thresholding layer for denoising in the Hadamard transform domain that improves adversarial noise suppression and prevents gradient-based attacks due to its non-differentiability;
3. A newly created dataset generated by applying first-order gradient attacks on various state-of-the-art CNN and transformer-based methods across haze, rain-streak, and snow removal scenarios.

Extensive experiments show that QHNet can defend a wide range of CNN and transformer models with a single set of weights without modifying the target models.

The structure of this paper is as follows: Section 2 reviews related works, Section 3 details the methodology and components of QHNet, Section 4 introduces the collected dataset of attacked/clean images, Section 5 presents a comparative analysis of our results against other methods, and Section 6 offers a summary of our findings.

II. RELATED WORK

A. Adversarial Attacks and Defenses

An adversarial example x_{adv} for a clean image x_c and a model \mathcal{M} is defined such that:

$$x_{adv} = x_c + \rho \quad (1)$$

where ρ is a small perturbation constrained by $d(x_c, x_{adv}) \leq \epsilon$ for some distance $d(\cdot, \cdot)$ and the model's output changes significantly $\mathcal{M}(x_{adv}) \neq \mathcal{M}(x_c)$. In the case of weather removal models, an adversarial example could cause an inability to remove the weather phenomenon, the introduction of artifacts, or severe damage to the processed image (Fig. 1).

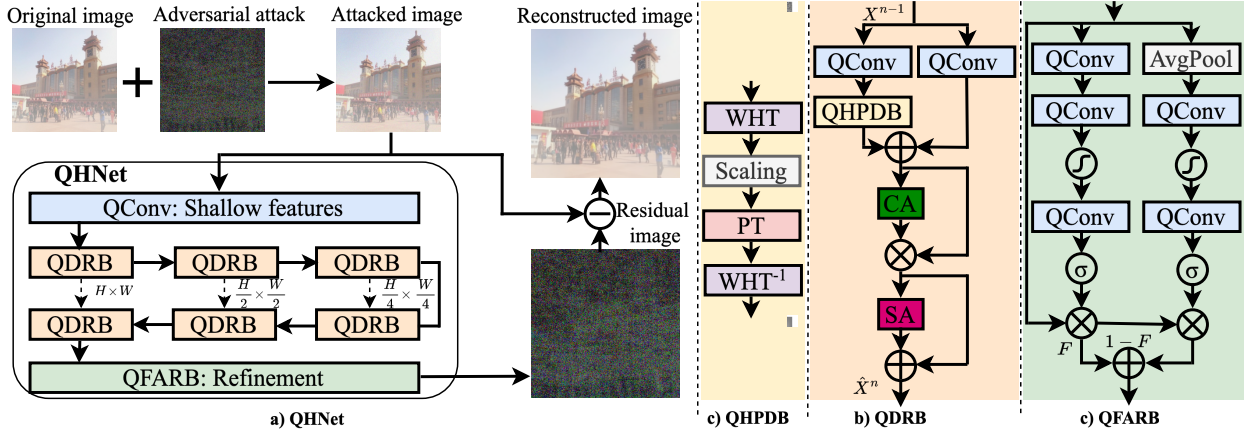


Fig. 2. QHNet mitigates adversarial attacks by first transforming the attacked input image into a quaternion representation. It then processes the image through an encoder-decoder architecture built with Quaternion Hadamard Residual Blocks (QDRB), incorporating spatial and channel attention mechanisms. Polynomial thresholding is applied to denoise in the frequency domain. Finally, the Quaternion Feature Aggregation and Refinement Block (QFARB) produces a perturbation-free image that is safe for further processing by the target model.

Defense strategies can be broadly categorized into retraining-based and non-retraining methods (Table I). Retraining-based methods, such as adversarial training or defensive distillation, incorporate adversarial examples into the training process to improve model robustness [12]. However, these methods are computationally expensive and often infeasible for real-time applications.

Non-retraining methods focus on preprocessing or modifying the input to mitigate the effect of adversarial perturbations without the model alteration. Misclassification Aware Adversarial Training (MART) differentiates between misclassified and correctly classified examples during training, significantly improving robustness [29]. JPEG compression reduces high-frequency signal components, effectively countering perturbations and enhancing model robustness against adversarial attacks [13].

Other input transformations, such as bit-depth reduction and total variance minimization, are used to preprocess inputs, making it difficult for adversaries to exploit the model [14]. Pixel deflection redistributes pixel values, introducing local noise that helps maintain classification accuracy in the presence of adversarial manipulations [15]. CIIDefence combines class-specific image inpainting with wavelet-based denoising, providing a non-differentiable layer that prevents gradient-based attacks [17]. Mustafa et al. proposed a computationally efficient image enhancement approach that leverages deep image restoration networks and superresolution techniques to mitigate adversarial perturbation effects [19]. Finally, Gui et al. explicitly address the defense of low-level image processing methods, highlighting a gap in research for this domain [4].

B. Deep Learning in the Transform Domain

Previous research has leveraged various orthogonal transforms such as the Discrete Fourier Transform, Discrete Cosine Transform (DCT), and wavelet transforms in deep learning. These transforms have been applied to feature

extraction, providing invariance to rotation and taking advantage of the convolutional theorem, which allows convolution operations in the transform domain to be performed as pointwise multiplications [30]. The Walsh-Hadamard Transform (WHT) has gained attention due to its real-valued nature and computational efficiency [31], [32].

One of the main advantages of the WHT is that it only involves additions and subtractions, with matrix W_N elements restricted to -1 and 1 . The fast algorithm, similar to the Fast Fourier Transform (FFT), reduces the computational complexity from $O(N^2)$ to $O(N \log N)$. The WHT's simplicity and efficiency make it an excellent choice for real-time applications with limited computational resources.

III. PROPOSED METHOD

In the following subsections, we first overview the proposed QHNet. Then, we introduce the polynomial thresholding (PT) algorithm, Quaternion Hadamard Denoising Convolutional Block (QHDCB), and Quaternion Denoising Residual Block (QDRB). Next, we describe the Quaternion Feature Aggregation and Refinement Block (QFARB). Finally, we discuss the training strategy and model optimization.

A. Image Data Representation and Processing

Quaternion numbers extend the concept of complex numbers to 4 dimensions and can be written as $q = a + bi + cj + dk$, where $a, b, c,$ and d are real numbers, and $i, j,$ and k follow these multiplication rules: $i^2 = j^2 = k^2 = ijk = -1$, $ij = k, ji = -k, ik = j, ki = -j$ [33]. The input image $I_{in} \in \mathbb{R}^{H \times W \times 3}$, with color channels (R, G, and B) and spatial dimensions $H \times W$ is encoded using a quaternion-valued matrix:

$$Q = 0 + Ri + Gj + Bk \quad (6)$$

where $R, G, B \in \mathbb{R}^{H \times W}$ are color channels of the image normalized in the range $[0, 1]$.

> REPLACE THIS LINE WITH YOUR MANUSCRIPT ID NUMBER (DOUBLE-CLICK HERE TO EDIT) <

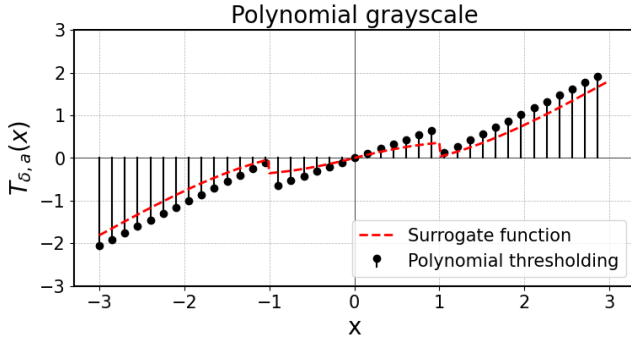


Fig. 3. Polynomial thresholding and surrogate function.

Properties of QNNs are defined not by the representation itself but by how quaternion values are processed. The Hamilton product is used for operations on quaternions. The product of two quaternions $p = p_r + p_i i + p_j j + p_k k$ and $q = q_r + q_i i + q_j j + q_k k$ is given by:

$$\begin{aligned} p \otimes q = & (p_r q_r - p_i q_i - p_j q_j - p_k q_k) \\ & + (p_r q_i + p_i q_r + p_j q_k - p_k q_j) i \\ & + (p_r q_j - p_i q_k + p_j q_r + p_k q_i) j \\ & + (p_r q_k + p_i q_j - p_j q_i + p_k q_r) k \end{aligned} \quad (7)$$

The quaternion convolution $\text{QConv}(Q, W)$ combines the Hamilton product applied pointwise with the usual sliding window operation:

$$(Q * W)_{(m,n)} = \sum_u \sum_v (Q_{(m+u,n+v)} \otimes W_{(u,v)}) \quad (8)$$

where $Q = Q_r + Q_i i + Q_j j + Q_k k$ and $W = W_r + W_i i + W_j j + W_k k$ are quaternion-valued matrices representing the input image and the filter weights, respectively. Here, m and n are the spatial coordinates of the output feature map, while u and v are the spatial coordinates of the filter kernel.

We use a split-activation function that operates independently on the components of the quaternion-valued feature map. Given a quaternion-valued feature map $Q = Q_r + Q_i i + Q_j j + Q_k k$, the split-activation function φ operates as follows:

$$Q = \varphi(Q_r) + \varphi(Q_i) i + \varphi(Q_j) j + \varphi(Q_k) k \quad (9)$$

where $\varphi(\cdot)$ is a real-valued activation function.

B. QHNet architecture

The proposed network architecture addresses adversarial attacks using a UNet-like encoding-decoding framework with skip connections (Fig. 3). We begin with a quaternion convolutional layer (QConv) with a 3×3 kernel to generate shallow features. These features are then processed by groups of K -stacked Quaternion Hadamard Residual Blocks (QHRBs) to create feature maps at full, half, and quarter resolutions. Each QHRB combines a quaternion convolutional layer and a QHPDB for feature extraction and transformation across spatial and frequency domains. This dual-domain processing helps differentiate the original signal from adversarial noise, allowing effective suppression via the PT layer. After decoding, the feature maps are refined by QFARB. The network reconstructs a residual image containing the estimated additive attack noise,

which is then subtracted from the original image to produce the final output with suppressed adversarial attack effects.

Polynomial Thresholding layer (PT): The polynomial thresholding layer is crucial as an activation function in the frequency domain. Typically, thresholding operators are used for denoising in the wavelet domain through the following steps: (1) orthogonal transform, (2) thresholding, and (3) inverse orthogonal transform. We adopt polynomial thresholding in the WHT domain, using surrogate gradients to achieve smooth gradients during the training phase for effective learning [34], [35]. The layer remains non-differentiable during inference, making the network resistant to gradient-based attacks. Polynomial thresholding generalizes commonly used soft and hard thresholds, providing more flexibility.

The polynomial thresholding operator $T_{\delta,a}(x)$ is defined as follows:

$$T_{\delta,a}(x) = \begin{cases} a_{N-1}x - a_N \text{sgn}(x)\delta & \text{if } |x| > \delta \\ \sum_{k=0}^{N-2} a_k x^{2k+1} & \text{if } |x| < \delta \end{cases} \quad (10)$$

Here, δ is the threshold, a is the vector of polynomial coefficients, N is the number of terms in the polynomial, and $\text{sgn}(x)$ is the sign function. The general form of the thresholding operator can be expressed in the matrix form:

$$T_{\delta,a}(x) = f(x) \cdot a \quad (11)$$

where $f(x) = [f_0(x), f_1(x), \dots, f_N(x)]$ is a vector of functions applied to the input x , defined as:

$$f(x) = \begin{cases} [0, 0, \dots, 0, x - \delta \text{sgn}(x)] & \text{if } |x| > \delta \\ [x, x^3, \dots, x^{2N-3}, 0, 0] & \text{if } |x| < \delta \end{cases} \quad (12)$$

An optimum solution for a can be found by solving the following optimization problem as follows:

$$a_{opt} = \arg \min_a \|d - W^T f(Y)a\| \quad (13)$$

where d is the desired attack-free image, a_{opt} is the optimal set of parameters a , W is the transform matrix, $Y = W \cdot y$ is the transformed version of the measured image. For an energy-preserving transform such as Welsh-Hadamard, this can be simplified to:

$$a_{opt} = \arg \min_a \|D - f(Y)a\| \quad (14)$$

where D is the transformed version of the desired signal d . When considering many observations, we can alternatively find the minimum MSE (MMSE) error across all the observations:

$$a_{opt} = E(f^T(Y)f(Y))^{-1} E(f^T(Y)D) \quad (15)$$

where $E(\cdot)$ represents the expected value estimation on the whole dataset. For grayscale images attacked with FGSM, $\delta = 1.0$, $N = 5$ we found $a = [0.707, 0.014, 0.008, 0.999, 0.940]$ (Fig. 4). During the training phase, we replace the hard threshold condition with a sigmoid function, introducing the following surrogate function:

$$T_{\delta,a}(x) = \sigma(|x| - \delta) a_{N-1} x - \sigma(|x| - \delta) a_N \text{sgn}(x) \delta + (1 - \sigma(|x| - \delta)) \sum_{k=0}^{N-2} a_k x^{2k+1} \quad (16)$$

where, σ denotes the sigmoid function, which replaces the traditional hard thresholding condition.

Algorithm 1 Polynomial Thresholding Layer

Require: Tensor $X \in \mathbb{R}^{B \times C \times H \times W}$, coefficients $a \in \mathbb{R}^N$, threshold $\delta \in \mathbb{R}^{C \times 1}$

- 1: Reshape X to $\mathbb{R}^{B \times C \times H \times W}$
- 2: Expand δ to $\delta' \in \mathbb{R}^{B \times C \times H \times W}$
- 3: Compute $|\hat{X}|$ and $\text{sgn}(\hat{X})$
- 4: $C = |\hat{X}| > \delta'$
- 5: Initialize $f_X \in \mathbb{R}^{B \times C \times H \times W \times N}$ to zeros
- 6: **for** each $i \in [1, H \times W]$ **do**
- 7: **if** $C[i]$ is True **then**
- 8: $f_X[i] = [0, 0, \dots, 0, \hat{X}[i] - \delta' \cdot \text{sgn}(\hat{X}[i])]$
- 9: **else**
- 10: $f_X[i] = [\hat{X}[i], \hat{X}[i]^3, \dots, \hat{X}[i]^{2N-3}, 0, 0, 0]$
- 11: **end if**
- 12: **end for**
- 13: $Y = f_X \cdot a^X$
- 14: Reshape Y back to $\mathbb{R}^{B \times C \times H \times W}$
- 15: **return** Y

The polynomial thresholding layer is presented in Algorithm 1 and operates by first reshaping the input tensor X of size $B \times C \times W \times H$ into size $B \times C \times W \cdot H$. The tensor of trainable thresholds δ is then expanded to match the dimensions of \hat{X} . Next, the absolute value $|\hat{X}|$ and the sign $\text{sgn}(\hat{X})$ of \hat{X} are computed. The condition tensor O is calculated, where each element is true if the corresponding element of \hat{X} exceeds the threshold δ . Polynomial terms are calculated based on whether the condition O is true or false: if true, the last two terms of f_x are set to \hat{X} and $-\delta \cdot \text{sgn}(\hat{X})$ respectively; if false, polynomial terms x^{2k+1} for k from 0 to $N - 2$ are computed and set.

The final output tensor Y is obtained by multiplying the matrix of polynomial terms f_x with the vector of polynomial coefficients a , and reshaping the result back to the original size $B \times C \times W \times H$.

Quaternion Hadamard Polynomial Denoising Block (QHPDB): The QHPDB is designed to effectively suppress adversarial noise by leveraging the Walsh-Hadamard Transform (WHT) and quaternion convolution. The process begins with applying the WHT to the input tensor and converting the data into the transform domain, where noise can be more easily identified and suppressed. For an input tensor $X \in \mathbb{R}^{B \times C \times H \times W}$, the 2D WHT is applied along the last two axes, resulting in $\hat{X} = \text{WHT}(X)$. Then, quaternion convolution $QConv$ with learnable kernel W_{st} is performed on \hat{X} to replace the scaling operation. The transformed and scaled tensor $\hat{X}_{st} = QConv(\hat{X}, W_{st})$ undergoes polynomial thresholding to attenuate high-frequency components $\tilde{Y} = PT(\hat{X}_{st})$. After thresholding, the inverse WHT is applied to bring the data back to the spatial domain, yielding the tensor $Y = \text{WHT}^{-1}(\tilde{Y})$.

Quaternion Denosing Residual Block (QDRB): The block begins with a Quaternion Convolution layer with a kernel size of 3×3 . The use of quaternion convolutions is particularly beneficial here as it can effectively handle the multidimensional nature of the data. Following the initial convolution, the data is passed through the QHPDB layer. Operating in the transform

domain using the Welsh-Hadamard Transform (WHT), the QHPD applies polynomial thresholding PT. An additional branch propagates the original features through a single quaternion convolution layer to ensure that essential image features are not lost during the denoising process. This facilitates the retention of essential details unaffected by the noise removal process. The block further incorporates Channel Attention and Spatial Attention mechanisms sequentially.

Channel Attention (CA): selects the most informative feature channels by computing a channel-wise attention map and multiplying it with the input features. The CA mechanism is mathematically represented as follows:

$$CA(X) = \sigma \left(QConv2 \left(\text{ReLU} \left(QConv1 \left(\text{AvgPool}(X) \right) \right) \right) \right) \quad (17)$$

where $\text{AvgPool}(X)$ is the adaptive average pooling operation, reducing each channel to a single value, $QConv1$ is a quaternion convolution layer reducing the number of channels by the reduction ratio, ReLU is the ReLU activation function, $QConv2$ is a quaternion convolution layer restoring the original number of channels, and σ is the sigmoid activation function producing the attention map.

Spatial Attention (SA): highlights significant spatial features by applying a series of convolutions and activations to enhance the regions of interest in the feature map. The SA mechanism is mathematically represented as follows:

$$SA(X) = \sigma \left(QConv3 \left(\text{ReLU} \left(QConv2 \left(QConv1(X) \right) \right) \right) \right) \quad (18)$$

where $QConv1$ is the first quaternion convolution layer with a kernel size of 3×3 , $QConv2$ is a second quaternion convolution layer reducing the number of channels, ReLU is the ReLU activation function, $QConv3$ is the final quaternion convolution layer restoring the original number of channels, and σ is the sigmoid activation function producing the attention map.

Finally, QDRB adds the input features back to the output. The whole process could be represented as follows:

$$\hat{H}_1^n = \text{QHPDB}(QConv1(X^{n-1}, W_1)) \quad (19)$$

$$\hat{H}_2^n = QConv2(X^{n-1}, W_2) \quad (20)$$

$$X^n = SA \left(CA(\hat{H}_1^n + \hat{H}_2^n) \right) + X^{n-1} \quad (21)$$

where X^{n-1} is the input to the n -th QDRB, \hat{H}_1^n and \hat{H}_2^n are intermediate feature maps processed through the QHPDB and an additional $QConv$ layer, respectively.

Quaternion Feature Aggregation and Refinement Block (QFARB): At the end of the processing, the feature map is adaptively refined following the procedure proposed in [39] and adapted for the quaternion case to robustly restore fine structural and textural details. The input features pass through a series of quaternion Convolution ($QConv$) layers, capturing complex inter-channel relationships efficiently. The output undergoes global average pooling (GAP) to condense spatial information, followed by additional $QConv$ layers and hyperbolic tangent (\tanh) activations to refine the features.

The attention map M is generated using a sigmoid activation function on another $QConv$ layer output. This map weighs the original and refined features, selecting the most informative parts.

TABLE II
SYNTHETIC HAZE REMOVAL RESULTS (RESIDE 6K DATASET)

Attack Method	Dehazing method	Original/Attacked		Superresolution		Denoising		QHNet	
		PSNR	SSIM	PSNR	SSIM	PSNR	SSIM	PSNR	SSIM
FGSM $\epsilon = 2$ $i = 1$	DehazeFormer [51]	26.208/20.954	0.954/0.898	21.094	0.893	21.051	0.904	22.830	0.921
	MixDehazeNet [37]	26.335/18.238	0.942/0.852	18.659	0.856	21.323	0.865	21.084	0.893
	FSNet [38]	27.231/19.607	0.947/0.873	19.844	0.874	22.476	0.872	22.076	0.900
	DSANet [39]	27.283/18.883	0.948/0.855	19.057	0.855	23.172	0.889	21.586	0.889
	Chen et al. [40]	29.284/22.557	0.970/0.915	23.176	0.920	25.366	0.924	26.031	0.952
I-FGSM $\epsilon = 5$ $i = 5$	DehazeFormer [51]	26.208/9.187	0.954/0.628	9.863	0.649	19.236	0.837	22.076	0.919
	MixDehazeNet [37]	26.335/8.268	0.942/0.570	8.690	0.589	18.085	0.817	21.320	0.893
	FSNet [38]	27.231/10.233	0.947/0.432	11.018	0.481	22.388	0.872	23.941	0.913
	DSANet [39]	27.283/13.031	0.948/0.717	13.427	0.729	22.236	0.868	23.604	0.907
	Chen et al. [40]	29.284/12.695	0.970/0.697	13.107	0.711	21.288	0.872	25.532	0.947
I-FGSM $\epsilon = 5$ $i = 10$	DehazeFormer [51]	26.208/7.728	0.954/0.570	8.343	0.592	19.873	0.842	23.692	0.932
	MixDehazeNet [37]	26.335/7.697	0.942/0.536	8.058	0.556	18.085	0.817	23.257	0.915
	FSNet [38]	27.231/6.752	0.947/0.167	7.348	0.206	22.414	0.869	24.873	0.922
	DSANet [39]	27.283/12.055	0.948/0.677	12.720	0.698	22.236	0.868	25.073	0.926
	Chen et al. [40]	29.284/10.962	0.970/0.623	11.586	0.651	20.835	0.854	27.237	0.957

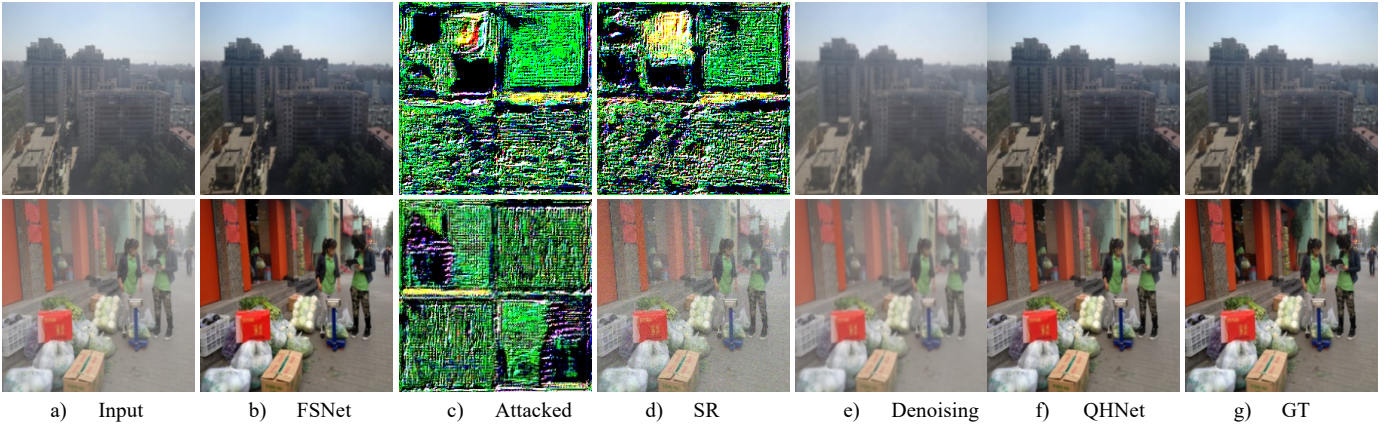


Fig. 4. Haze removal by FSNet method on Reside6k dataset. With I-FGSM attack, $\epsilon = 5$, $i = 5$. a) Input image b) FSNet without attack. FSNet performs well. c) FSNet on attacked image. Severe artifacts damage all 3 images. d) Superresolution can prevent artifacts in 2 out of 3 cases, but FSNet can still not remove the haze. e) Denoising prevents artifacts in all 3 cases, but FSNet can still not remove the haze. f) QHNet leads to the successful removal of haze on all 3 images. g) Provides ground truth for comparison.

The final output \hat{Y} is computed as a weighted sum of these features, preserving essential details while enhancing image quality. The process within the QFARB is described by:

$$\hat{M}_1^n = \tanh\left(\text{QConv}\left(\text{QConv}\left(\text{GAP}(Y)\right)\right)\right) \quad (22)$$

$$\hat{M}_2^n = \tanh\left(\text{QConv}\left(\text{QConv}(Y)\right)\right) \quad (23)$$

$$\hat{Y} = Y \odot \hat{M}_2 + (1 - \hat{M}_2) \odot \hat{M}_1 \quad (24)$$

where, \hat{M}_1 is the refined feature map, \hat{M}_2 is the attention map, and \hat{Y} is the final output feature.

V. DATASET

To evaluate and train the QHNet, we have collected a custom dataset AWCVD covering diverse adverse weather conditions, including haze, rain, and snow. Our dataset was built by attacking images sampled from various synthetic datasets on different state-of-the-art models.

For dehazing, we attacked DehazeFormer [51], MixDehazeNet [37], FSNet [38], DSANet [39], and Chen et al. [40] on RESIDE-6K [41] dataset. For rain-streak removal, we targeted M3SNet [42], Restormer [43], UDR-S2Former [44], and Chen et al. [40] on Rain-13k [45] dataset. For snow removal, we

attacked DSANet [39], OKNet [50], and Chen et al. [40] on the CSD dataset [46]. These models were trained on the respective datasets and selected to represent a combination of CNN- and transformer-based approaches, ensuring a comprehensive evaluation.

Methods: We employed the Fast Gradient Sign Method (FGSM) and its iterative version (I-FGSM) as our first-order gradient methods to produce adversarial examples [6], [47]. Attack involves a loss function $\mathcal{L}(x_c + \rho, y_c; \theta)$, where θ denotes the network parameters. The aim is to maximize this loss by solving:

$$\mathcal{L} \arg \max_{\rho \in R^m} \mathcal{L}(x_c + \rho, y_c; \theta) \quad (25)$$

FGSM achieves this in a single step by determining adversarial perturbations. It does so by moving in the direction opposite to the gradient of the loss function with respect to the input (∇):

$$x_{\text{adv}} = x_c + \epsilon \cdot \text{sign}(\nabla \mathcal{L}(x_c, y_c; \theta)) \quad (26)$$

where, ϵ represents the step size, which effectively bounds the l_∞ norm of the perturbation.

I-FGSM applies the perturbation iteratively with the update rule:

$$x_{m+1} = \text{clip}\left(x_m + \alpha \cdot \text{sign}(\nabla \mathcal{L}(x_m, y_c; \theta))\right) \quad (27)$$

TABLE III
HEAVY RAIN REMOVAL RESULTS (RAIN100H DATASET)

Attack Method	Rain-removal method	Original/Attacked		Super-resolution		Denoising		QHNet	
		PSNR	SSIM	PSNR	SSIM	PSNR	SSIM	PSNR	SSIM
FGSM $\epsilon = 2$ $i = 1$	M3Snet [42]	29.307/28.135	0.928/0.920	27.552	0.909	18.916	0.716	28.572	0.923
	Restormer [43]	29.584/28.024	0.932/0.923	27.824	0.914	18.741	0.694	28.861	0.928
	Udr-s2former [44]	19.486/19.505	0.753/0.750	19.315	0.748	15.887	0.611	19.606	0.752
	Chen et al. [40]	25.929/25.216	0.886/0.876	25.064	0.872	18.147	0.673	25.582	0.882
I-FGSM $\epsilon = 5$ $i = 5$	M3Snet [42]	29.307/18.195	0.928/0.801	20.111	0.836	18.972	0.715	25.253	0.905
	Restormer [43]	29.584/18.797	0.932/0.805	20.734	0.844	18.691	0.722	26.504	0.916
	Udr-s2former [44]	19.486/17.506	0.753/0.673	17.743	0.683	15.974	0.606	18.844	0.714
	Chen et al. [40]	25.929/18.447	0.886/0.764	19.433	0.791	17.809	0.690	23.622	0.866
I-FGSM $\epsilon = 5$ $i = 10$	M3SNet [42]	29.307/14.547	0.928/0.690	16.833	0.764	18.643	0.700	26.211	0.909
	Restormer [43]	29.584/15.194	0.932/0.703	18.073	0.790	18.691	0.722	27.220	0.919
	Udr-s2former [44]	19.486/15.610	0.753/0.605	16.061	0.624	15.698	0.592	18.761	0.713
	Chen et al. [40]	25.929/15.036	0.886/0.635	16.447	0.698	17.517	0.680	24.020	0.869

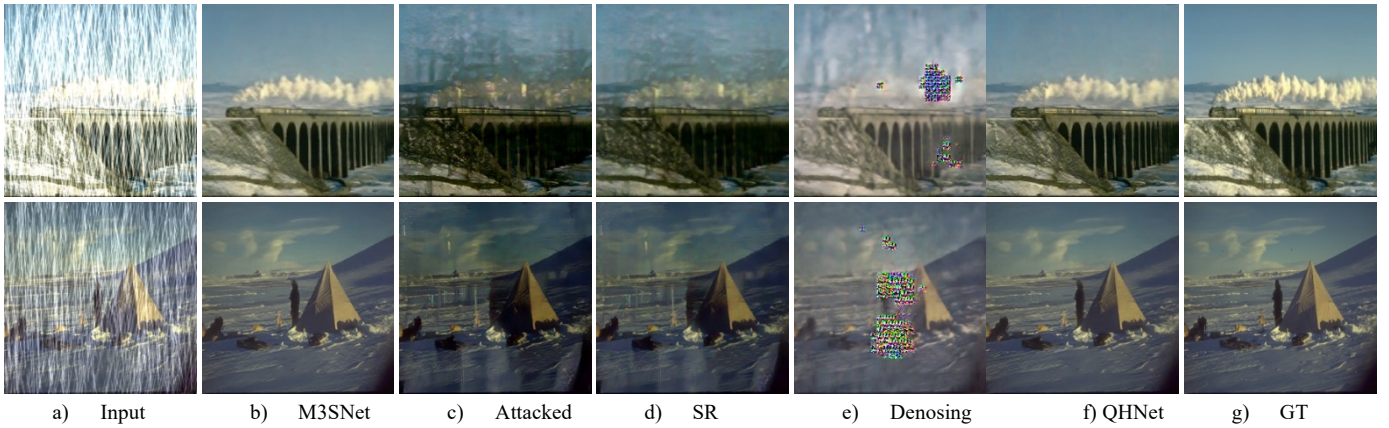


Fig. 5. Rain-streak removal by M3SNet on Rain100H dataset. With I-FGSM attack, $\epsilon = 5$, $i = 10$. a) input image b) M3SNet non-attacked input image c) M3SNet on attacked image: failing to remove streaks, with added artifacts. d) superresolution and e) denoising do not improve the situation significantly. f) QHNet reduces effects of attack. g) Ground truth.

where m ranges from 0 to M , with $x_0 = x_c$. After M iterations, the final adversarial example is $x_{adv} = x_M$.

We use different combinations of ϵ (2, 4, 6, 8, 10, and 15) and iteration counts ($i = 1, 3, 5, 7$, and 11) to attack the selected models. This approach enabled us to generate various adversarial examples paired with their clean counterparts for training our defense model. In total, we sampled 11,190 images for training, distributed as follows: 3000 from Rain-13k, 5000 from RESIDE-6K, and 3190 from CSD. For testing, we sampled 2100 images from the same "train" split of the original dataset, distributed as follows: 600 from Rain-13k, 1000 from RESIDE-6K, and 500 from CSD.

All the images were resized to the size of the Test split of the dataset, which is used only for validation during training and in ablation studies. The actual efficiency of the defense technique should be evaluated using the testing datasets accompanying the original datasets and the attack on the target model.

IV. EXPERIMENTS

A. Experimental procedures

We evaluate the performance of QHNet to defend against adversarial attacks on three low-level computer vision tasks: haze

removal, rain-streak removal, and snow removal. We have attacked recent weather removal methods using FGSM (epsilon=2), I-FGSM (epsilon=5, iterations=10), and I-FGSM (epsilon=5, iterations=10). Attacked images were processed by QHNet, by superresolution technique ESRGAN [48], and by state-of-the-art denoising method KBNNet [49]. Then, we applied the target method to the original attacked image, and the images were processed with QHNet, ESRGAN, and KBNNet.

Measuring defense efficiency: We measured the quality of restoration using PSNR and SSIM, common metrics for checking image quality. The results are presented in Tables II-IV and Figures 4-6. For dehazing, we attacked DehazeFormer [51], MixDehazeNet [37], FSNet [38], DSANet [39], and Chen et al. [40] on RESIDE-6K [41] dataset. For rain-streak removal, we targeted M3SNet [42], Restormer [43], UDR-S2Former [44], and Chen et al. [40] on Rain-13k [45] dataset. For snow removal, we attacked DSANet [39], OKNet [51], and Chen et al. [40].

B. Implementation details

The model is trained on 64x64 image patches, leveraging the AdamW optimizer with parameters $\beta_1 = 0.9$, $\beta_2 = 0.999$, and $\epsilon = 1 \times 10^{-8}$.

> REPLACE THIS LINE WITH YOUR MANUSCRIPT ID NUMBER (DOUBLE-CLICK HERE TO EDIT) <

TABLE IV
SNOW REMOVAL RESULTS (CSD DATASET)

Attack method	Rain-removal method	Original results and attack		Superresolution		Denoising		QHNet	
		PSNR	SSIM	PSNR	SSIM	PSNR	SSIM	PSNR	SSIM
FGSM $\epsilon=2$ $i=1$	DSANet [39]	29.038/13.304	0.941/0.669	14.519	0.697	22.343	0.859	28.491	0.935
	OKNet [50]	29.084/12.359	0.942/0.407	17.250	0.741	22.979	0.843	24.626	0.828
	Chen et al. [40]	26.749/21.277	0.920/0.868	22.008	0.879	23.702	0.883	23.826	0.899
I-FGSM $\epsilon=5$ $i=5$	DSANet [39]	29.038/8.659	0.941/0.222	12.013	0.452	18.579	0.799	28.470	0.936
	OKNet [50]	29.084/5.470	0.942/0.015	5.477	0.015	21.457	0.833	24.624	0.829
	Chen et al. [40]	26.749/14.042	0.920/0.717	14.208	0.728	18.697	0.824	24.303	0.901
I-FGSM $\epsilon=5$ $i=10$	DSANet [39]	29.038/7.369	0.941/0.142	11.184	0.387	17.615	0.781	28.527	0.936
	OKNet [50]	29.084/5.469	0.942/0.015	5.472	0.015	21.002	0.814	24.638	0.829
	Chen et al. [40]	26.749/13.049	0.920/0.677	13.344	0.693	17.552	0.801	25.679	0.911



a) Input b) Chen et al. c) Attacked d) SR e) Denoising f) QHNet g) GT

Fig. 6. Snow removal by Chen et al. on Rain100H dataset. With I-FGSM attack, $\epsilon = 5, i = 5$. a) Input image b) non-attacked image restored by Chen et al., c) attacked image restored by Chen et al. with severe artifacts or unremoved snowflakes. d) Superresolution and denoising e) improve quality but introduce artifacts and darken the image f) QHNet successfully removes snowflakes, producing images close to the ground truth g) ground truth.

The learning rate is set to an initial value of 1×10^{-3} , decaying to a minimum of 1×10^{-7} through a cosine annealing schedule with a warm-up phase of 2 epochs. This training strategy ensures a smooth and effective learning process. The training process spans 250 epochs with a batch size 12, conducted on a single NVIDIA A100 GPU. We use the Structural Similarity Index (SSIM) loss function:

$$\mathcal{L} = 1 - \text{SSIM}(QHNet(X), Y) \quad (25)$$

where $QHNet(\cdot)$ is the proposed network, X represents the attacked input image, and Y is the ground truth image.

C. Experimental results

In this subsection, we discuss the effectiveness of QHNet in protection against adversarial attacks.

Haze removal: Table II and Figure 4 present results for attacking haze removal methods: DehazeFormer, MixDehazeNet, FSNet, DSANet, and Chen et al. For haze removal techniques, even FGSM with epsilon=2 significantly reduces performance (PSNR from 26.208 to 20.954, and SSIM from 0.954 to 0.898 for DehazeFormer). Superresolution introduces artifacts and generally offers insignificant improvement. Denoising performs better, but QHNet significantly improves the performance of the target model on attacked images. Performance of all dehazing methods is severely affected by I-FGSM attack with epsilon=5 and i=10. For

example, for Chen et al., PSNR degrades from 29.284 to 10.962 and SSIM from 0.970 to 0.623. QHNet restores PSNR to 27.237 and SSIM to 0.957, which is lower than performance without attack but reasonable for subsequent computer vision applications and significantly better than denoising and superresolution improvements. They remove rain effectively.

Rain-streak removal: Table III and Figure 5 demonstrate the attack on various rain-streak removal methods (M3SNet, Restormer, UDR-S2Former, Chen, et al.) for heavy rain on the Rain100H dataset. Light attacks (epsilon=2) do not significantly impact performance, but severe attacks (epsilon=5, i=10) drastically reduce performance. From ~ 30 PSNR to ~ 15 PSNR, both superresolution and denoising fail to prevent degradation of rain-streak removal performance and introduction of artifacts. QHNet significantly reduces degradation, especially in the case of DSANet.

Snow removal: Table IV and Figure 6 present snow removal results. Methods like DSANet and OKNet work well under normal conditions but degrade significantly under FGSM (epsilon=2) attacks. Superresolution and denoising methods do not fully fix the damage and often add artifacts. QHNet achieves the highest PSNR and SSIM scores, recovering attacked images effectively. Overall, superresolution and denoising methods do not fully repair damage and often introduce artifacts. QHNet consistently achieves the highest PSNR and SSIM scores,

> REPLACE THIS LINE WITH YOUR MANUSCRIPT ID NUMBER (DOUBLE-CLICK HERE TO EDIT) <

effectively recovering attacked images.

D. Ablation study

In this section, we analyze the effectiveness of the components of the proposed architecture QHNet. The "Real" network, which serves as the baseline, has the same architecture as QHNet but does not utilize the quaternion approach. It contains 16.8 million parameters and shows lower performance in both PSNR (43.1448) and SSIM(0.9894) compared to QHNet.

TABLE IV
ABLATION STUDY ON THE COMPONENTS OF THE PROPOSED
ARCHITECTURE QHNET

QHPDB	QFARB	Attention	PT	#params	PSNR	SSIM
×	✓	✓	✓	4,576,392	43.2330	0.9907
✓	×	✓	✓	3,649,296	42.8338	0.9899
✓	✓	×	✓	2,648,498	42.8358	0.9890
✓	✓	✓	×	3,676,104	43.2343	0.9907
✓	✓	✓	✓	3,676,104	43.3087	0.9934

As shown in Table IV, removing any component from QHNet results in a drop in performance, confirming the contribution of each module. QHNet, which includes all components (QHPDB, QFARB, Attention, and PT), achieves the best results with a PSNR of 43.3087 and an SSIM of 0.9934, demonstrating the effectiveness of integrating all these developed modules.

V. CONCLUSION

This paper introduces the Quaternion-Hadamard Network (QHNet) as a novel, model-agnostic defense strategy against first-order white-box adversarial attacks. It addresses a critical vulnerability in recent deep-learning methods for removing rain, snow, and haze, which remain highly susceptible to adversarial attacks despite their effectiveness in improving image quality under adverse weather conditions. Unlike traditional defenses such as adversarial training and model distillation, which often require extensive retraining and have high computational costs, QHNet offers a more practical solution. It efficiently reduces adversarial noise using the Quaternion Hadamard Denoising Convolutional Block (QHDCB) and the Quaternion Denoising Residual Block (QDRB), which leverages polynomial thresholding. These components are integrated into an encoder-decoder architecture, followed by feature refinement, to enhance the robustness of low-level computer vision models without the need for costly retraining or high computational overhead. Through extensive computer simulations, QHNet has demonstrated robust defense capabilities against adversarial attacks across various scenarios, including haze removal, rain-streak removal, and snow removal, as validated by metrics such as PSNR and SSIM. Additionally, our analysis emphasizes the detrimental effects of adversarial attacks on dehazing methods and their subsequent impact on object detection performance. To support further research, we introduce the Adversarial Weather Conditions Vision Dataset (AWCVD), a novel dataset containing adversarially perturbed weather-condition images designed to evaluate model robustness.

In future research, we aim to explore the generalizability of our approach across various applications and attack modes, with a particular focus on black-box and gray-box attacks. Additionally, we plan to develop new dataset-based adversarial attacks by leveraging machine learning, deep learning, and feature optimization techniques. This will provide us with deeper insights into the broader applicability and potential limitations of QHNet, including its performance in probabilistic scenarios. By understanding these dynamics, we can further refine QHNet, developing more robust, adaptable, and versatile defense mechanisms for a wide range of image processing models. We also plan to incorporate the Quaternion Probabilistic Network (QPN) concept. This neural network combines quaternion-based processing for handling multidimensional data with probabilistic mechanisms to account for uncertainty. This approach would enable more efficient, robust, and flexible models, particularly when data complexity and uncertainty are intertwined. By integrating probabilistic reasoning with the inherent advantages of quaternion-based processing, we aim to significantly improve QHNet's resilience to adversarial attacks and enhance its overall performance in complex, real-world environments.

REFERENCES

- [1] J. Xiao, et al., "Image De-Raining Transformer," *IEEE Trans. Pattern Anal. Mach. Intell.*, vol. 45, no. 11, pp. 12978-12995, 2023.
- [2] H. Kuang, H. Liu, Y. Wu and R. Ji, "Semantically Consistent Visual Representation for Adversarial Robustness," in *IEEE Transactions on Information Forensics and Security*, vol. 18, pp. 5608-5622, 2023.
- [3] M. Zhou, et al., "Adversarial Attack and Defense in Deep Ranking," *IEEE Trans. Pattern Anal. Mach. Intell.*, vol. 46, no. 8, pp. 5306-5324, 2024.
- [4] J. Gui et al., "Fooling the image dehazing models by first order gradient," *IEEE Trans. Circuits Syst. Video Technol.*, pp. 6265-6278, 2024.
- [5] X. Hu, S. Li, Q. Ying, W. Peng, X. Zhang and Z. Qian, "Establishing Robust Generative Image Steganography via Popular Stable Diffusion," in *IEEE Transactions on Information Forensics and Security*, vol. 19, pp. 8094-8108, 2024.
- [6] A. Yazdinejad, A. Dehghantanha, H. Karimipour, G. Srivastava and R. M. Parizi, "A Robust Privacy-Preserving Federated Learning Model Against Model Poisoning Attacks," in *IEEE Transactions on Information Forensics and Security*, vol. 19, pp. 6693-6708, 2024.
- [7] A. Madry, et al., "Towards deep learning models resistant to adversarial attacks," in *Proc. ICLR*, 2018.
- [8] S. M. Moosavi-Dezfooli, et al., "Universal adversarial perturbations," in *Proc. IEEE Conf. Comput. Vis. Pattern Recognit. (CVPR)*, 2017.
- [9] Y. Wang, T. Sun, X. Yuan, S. Li and W. Ni, "Minimizing Adversarial Training Samples for Robust Image Classifiers: Analysis and Adversarial Example Generator Design," in *IEEE Transactions on Information Forensics and Security*, vol. 19, pp. 9613-9628, 2024.
- [10] A. Aldahdooh, et al., "Reveal of vision transformers robustness against adversarial attacks," Jun. 2021, arXiv:2106.03734. [Online]. Available: <https://arxiv.org/abs/2106.03734>.
- [11] K. Mahmood et al., "On the robustness of vision transformers to adversarial examples," in *Proc. IEEE/CVF Int. Conf. Comput. Vis.*, 2021, pp. 7818-7827.
- [12] M. Esmailpour, P. Cardinal and A. L. Koerich, "Multidiscriminator Sobolev Defense-GAN Against Adversarial Attacks for End-to-End Speech Systems," in *IEEE Transactions on Information Forensics and Security*, vol. 17, pp. 2044-2058, 2022.
- [13] N. Das et al., "Keeping the bad guys out: Protecting and vaccinating deep learning with jpeg compression," May 2017, arXiv:1705.02900. [Online]. Available: <https://arxiv.org/abs/1705.02900>
- [14] C. Guo et al., "Countering adversarial images using input transformations," in *Proc. Int. Conf. Learn. Represent.*, Vancouver, BC, Canada, 2018, pp. 1-12.

> REPLACE THIS LINE WITH YOUR MANUSCRIPT ID NUMBER (DOUBLE-CLICK HERE TO EDIT) <

- [15] A. Prakash et al., "Deflecting adversarial attacks with pixel deflection," in Proc. IEEE Conf. Comput. Vis. Pattern Recognit., Jun. 2018, pp. 8571–8580.
- [16] P. Gupta and E. Rahtu, "Ciiddefence: Defeating adversarial attacks by fusing class-specific image inpainting and image denoising," in ICCV, 2019.
- [17] G. K. Dziugaite, Z. Ghahramani, and D. M. Roy, "A study of the effect of JPG compression on adversarial images," 2016, arXiv:1608.00853. [Online]. Available: <https://arxiv.org/abs/1608.00853>
- [18] Y. Wang et al., "Binary thresholding defense against adversarial attacks," *Neurocomputing*, vol. 445, pp. 61–71, 2021.
- [19] A. Mustafa et al., "Image Super-Resolution as a Defense Against Adversarial Attacks," *IEEE Trans. Image Process.*, vol. 29, pp. 1711–1724, 2020.
- [20] K. Bhardwaj et al., "Super-Efficient Super Resolution for Fast Adversarial Defense at the Edge," in 2022 Design, Automation & Test in Europe Conf. & Exhibition (DATE), Antwerp, Belgium, 2022, pp. 418–423.
- [21] M.-H. Guo et al., "Attention mechanisms in computer vision: A survey," *Comput. Visual Media*, vol. 8, pp. 331–368, 2022.
- [22] M. Uliceny, V. A. Krylov, and R. Dahyot, "Harmonic convolutional networks based on discrete cosine transform," *Pattern Recognit.*, vol. 129, 2022.
- [23] M. K. Patrick et al., "Capsule networks—A survey," *J. King Saud Univ.-Comput. Inf. Sci.*, 2019. [Online]. Available: <https://www.sciencedirect.com/science/article/pii/S1319157819309322>
- [24] C. Yuan and S. S. Agaian, "A comprehensive review of binary neural network," *Artif. Intell. Rev.*, vol. 56, no. 11, pp. 12949–13013, 2023.
- [25] Z. Wang, et al., "Learning Channel-Wise Interactions for Binary Convolutional Neural Networks," *IEEE Trans. Pattern Anal. Mach. Intell.*, vol. 43, no. 10, pp. 3432–3445, 2021.
- [26] A. Grigoryan and S. Agaian, *Quaternion and Octonion Color Image Processing with MATLAB*. Bellingham, WA, USA: SPIE Press, 2018.
- [27] C. J. Gaudet and A. S. Maida, "Deep quaternion networks," in Proc. Int. Joint Conf. Neural Netw. (IJCNN), Jul. 2018, pp. 1–8.
- [28] S. Agaian et al., *Hadamard Transforms*. Bellingham, WA, USA: SPIE Press, 2011.
- [29] Y. Wang et al., "Improving adversarial robustness requires revisiting misclassified examples," in Proc. ICLR, 2019, pp. 1–14.
- [30] M. Uteuliyeva, et al., "Fourier neural networks: A comparative study," *Intell. Data Anal.*, vol. 24, no. 5, pp. 1107–1120, 2020.
- [31] T. C. Deveci et al., "Energy efficient Hadamard neural networks," 2018, arXiv:1805.05421. [Online]. Available: <http://arxiv.org/abs/1805.05421>
- [32] H. Pan et al., "Deep neural network with Walsh–Hadamard transform layer for ember detection during a wildfire," in Proc. IEEE/CVF Conf. Comput. Vis. Pattern Recognit. Workshops (CVPRW), Jun. 2022, pp. 256–265.
- [33] A. M. Grigoryan and S. S. Agaian, "Retooling of color imaging in the quaternion algebra," *MathSJ*, vol. 1, no. 3, pp. 23–39, 2014.
- [34] C. B. Smith et al., "A wavelet-denoising approach using polynomial threshold operators," *IEEE Signal Process. Lett.*, vol. 15, no. 12, pp. 906–909, 2008.
- [35] E. O. Neftci et al., "Surrogate Gradient Learning in Spiking Neural Networks: Bringing the Power of Gradient-Based Optimization to Spiking Neural Networks," *IEEE Signal Process. Mag.*, vol. 36, no. 6, pp. 51–63, 2019.
- [36] Y. Zheng et al., "Curricular contrastive regularization for physics-aware single image dehazing," in Proc. IEEE/CVF Conf. Comput. Vis. Pattern Recognit. (CVPR), Jun. 2023, pp. 5785–5794.
- [37] L. Lu et al., "MixDehazeNet: Mix structure block for image dehazing network," 2023, arXiv:2305.17654. [Online]. Available: <http://arxiv.org/abs/2305.17654>
- [38] Y. Cui et al., "Image Restoration via Frequency Selection," *IEEE Trans. Pattern Anal. Mach. Intell.*, vol. 46, no. 2, pp. 1093–1108, 2024.
- [39] Y. Cui and A. Knoll, "Dual-domain strip attention for image restoration," *Neural Netw.*, vol. 171, pp. 429–439, 2024.
- [40] W.-T. Chen et al., "Learning multiple adverse weather removal via two-stage knowledge learning and multi-contrastive regularization: Toward a unified model," in Proc. IEEE/CVF Conf. Comput. Vis. Pattern Recognit., 2022, pp. 17653–17662.
- [41] C. O. Ancuti et al., "NH-HAZE: An image dehazing benchmark with non-homogeneous hazy and haze-free images," in Proc. IEEE/CVF Conf. Comput. Vis. Pattern Recognit. Workshops (CVPRW), Jun. 2020, pp. 444–445.
- [42] H. Gao et al., "A mountain-shaped single-stage network for accurate image restoration," 2023, arXiv:2305.05146. [Online]. Available: <http://arxiv.org/abs/2305.05146>
- [43] S. W. Zamir, et al., "Restormer: Efficient transformer for high-resolution image restoration," in Proc. IEEE/CVF Conf. Comput. Vis. Pattern Recognit. (CVPR), 2022.
- [44] S. Chen et al., "Sparse sampling transformer with uncertainty-driven ranking for unified removal of raindrops and rain streaks," in Proc. IEEE/CVF Int. Conf. Comput. Vis., 2023, pp. 13106–13117.
- [45] K. Jiang et al., "Multi-scale progressive fusion network for single image deraining," in Proc. IEEE/CVF Conf. Comput. Vis. Pattern Recognit., 2020, pp. 8343–8352.
- [46] W.-T. Chen et al., "All snow removed: Single image desnowing algorithm using hierarchical dual-tree complex wavelet representation and contradict channel loss," in Proc. IEEE/CVF Int. Conf. Comput. Vis., 2021, pp. 4196–4205.
- [47] A. Kurakin et al., "Adversarial machine learning at scale," in Proc. Int. Conf. Learn. Represent. (ICLR), 2017, pp. 1–17.
- [48] X. Wang et al., "ESRGAN: Enhanced super-resolution generative adversarial networks," in Proc. Eur. Conf. Comput. Vis. Workshops, 2018, pp. 63–79.
- [49] Y. Zhang et al., "KBNNet: Kernel basis network for image restoration," *CoRR*, 2023. [Online]. Available: <https://arxiv.org/abs/2303.02881>
- [50] Y. Cui, W. Ren, and A. Knoll, "Omni-Kernel Network for Image Restoration," in Proc. AAAI Conf. Artif. Intell., vol. 38, no. 2, pp. 1426–1434, 2024.
- [51] Y. Song, et al., "Vision Transformers for Single Image Dehazing," *IEEE Trans. on Image Processing*, vol. 32, pp. 1927–1941, 2023.



Vladimir Frants received a bachelor's degree (BC) in electrical engineering from the South Russian University of Economics and service, Russia, in 2011 and an MS degree in electrical engineering from the Don State Technical University, Russia, in 2013. He is pursuing a Ph.D. in computer science with The Graduate Center CUNY, USA. His current research interests include artificial intelligence, computer vision, image processing, and machine learning.



Sos S. Agaian, (Fellow, IEEE) is a Distinguished Professor with The City University of New York/CSI. His research interests include computational vision, machine learning, multimedia security, multimedia analytics, biologically inspired image processing, multi-modal biometrics, information processing, image quality, and biomedical imaging. He has authored over 850 technical articles and ten books in these areas. He is also listed as a co-inventor on 54 patents/disclosures. The technologies he invented have been adopted by multiple institutions, including the US Government, and commercialized by industry. He is a fellow of SPIE, IS&T, AAI, and AAAS. He received the Maestro Educator of the Year, sponsored by the Society of Mexican American Engineers. He received the Distinguished Research Award at The University of Texas at San Antonio. He received the Innovator of the Year Award in 2014, the Tech Flash Titans-Top Researcher Award (San Antonio Business Journal) in 2014, and the Entrepreneurship Award (UTSA-2013 and 2016). He was an Editorial Board Member for the Journal of Pattern Recognition and Image Analysis and an Associate Editor for several journals, including the IEEE Transactions On Image Processing. Currently, He is Associate Editor On IEEE Transactions. Systems, Man, Cybernetics and Journal of Electronic Imaging (IS&T and SPIE).